The ASAS-SN catalogue of variable stars – IV. Periodic variables in the APOGEE survey

Michał Pawlak [1]⋆ O. Pejcha [1]⋆ P. Jakubčík,[1,2] T. Jayasinghe,[3,4] C. S. Kochanek,[3,4] K. Z. Stanek,[3,4] B. J. Shappee,[5] T. W.-S. Holoien [6] Todd A. Thompson,[3,4,7] J. L. Prieto,[8,9] S. Dong,[10] J. V. Shields,[3] G. Pojmanski,[11] C. A. Britt[12] and D. Will[3,12]

[1] *Institute of Theoretical Physics, Faculty of Mathematics and Physics, Charles University in Prague, 180 00 Prague, Czech Republic*
[2] *New College, University of Oxford, Holywell Street, Oxford OX1 3BN, UK*
[3] *Department of Astronomy, The Ohio State University, 140 West 18th Avenue, Columbus, OH 43210, USA*
[4] *Center for Cosmology and Astroparticle Physics, The Ohio State University, 191 W. Woodruff Avenue, Columbus, OH 43210, USA*
[5] *Institute for Astronomy, University of Hawaii, 2680 Woodlawn Drive, Honolulu, HI 96822, USA*
[6] *Carnegie Observatories, 813 Santa Barbara Street, Pasadena, CA 91101, USA*
[7] *Institute for Advanced Study, Princeton, NJ 08540, USA*
[8] *Núcleo de Astronomía de la Facultad de Ingeniería y Ciencias, Universidad Diego Portales, Av. Ejército 441, Santiago, Chile*
[9] *Millennium Institute of Astrophysics, Santiago, Chile*
[10] *Kavli Institute for Astronomy and Astrophysics, Peking University, Yi He Yuan Road 5, Hai Dian District, China*
[11] *Warsaw University Observatory, Al Ujazdowskie 4, 00-478 Warsaw, Poland*
[12] *ASC Technology Services, 433 Mendenhall Laboratory, 125 South Oval Mall, Columbus, OH 43210, USA*

ABSTRACT

We explore the synergy between photometric and spectroscopic surveys by searching for periodic variable stars among the targets observed by the Apache Point Observatory Galactic Evolution Experiment (APOGEE) using photometry from the All-Sky Automated Survey for Supernovae (ASAS-SN). We identified 1924 periodic variables among more than 258 000 APOGEE targets; 465 are new discoveries. We homogeneously classified 430 eclipsing and ellipsoidal binaries, 139 classical pulsators (Cepheids, RR Lyrae, and δ Scuti), 719 long-period variables (pulsating red giants), and 636 rotational variables. The search was performed using both visual inspection and machine learning techniques. The light curves were also modelled with the damped random walk stochastic process. We find that the median [Fe/H] of variable objects is lower by 0.3 dex than that of the overall APOGEE sample. Eclipsing binaries and ellipsoidal variables are shifted to a lower median [Fe/H] by 0.2 dex. Eclipsing binaries and rotational variables exhibit significantly broader spectral lines than the rest of the sample. We make ASAS-SN light curves for all the APOGEE stars publicly available and provide parameters for the variable objects.

Key words: catalogues – surveys – stars: variables: general.

1 INTRODUCTION

Stellar variability is an important field of study in modern astronomy. Pulsating variable stars like Cepheids or RR Lyrae stars can be used as distance indicators thanks to the relations between the luminosity and the pulsational period (Leavitt 1908; Shapley 1931; Soszyński et al. 2008, 2009; Matsunaga, Feast & Soszyński 2011; Storm et al. 2011). Similar period–luminosity relations exist for close binary star systems (Rucinski 1994, 2004; Pawlak 2016). Photometry and spectroscopy for detached binary stars can provide

precise physical parameters for their individual components, which can be used to infer very accurate distances (Pietrzyński et al. 2011, 2013; Graczyk et al. 2014; Hełminiak et al. 2015). Furthermore, many types of variable stars, especially those providing distance estimates, trace different stellar populations, which makes them a perfect tool for studying the structure of the Milky Way (e.g. Dambis et al. 2015; Pietrukowicz et al. 2015; Skowron et al. 2018) and the galaxies within the Local Group (e.g. Pejcha & Stanek 2009; Haschke, Grebel & Duffau 2012; Deb & Singh 2014; Jacyszyn-Dobrzeniecka et al. 2017).

In recent years, large photometric sky surveys have dramatically increased the number of known variable stars. For example, the Optical Gravitational Lensing Experiment (OGLE; Udalski,

⋆ E-mail: michal.pawlak@utf.mff.cuni.cz

Szymański & Szymański 2015) has produced a collection of $\sim 10^6$ variable stars in some of the most crowded regions of the sky (Soszyński et al. 2014, 2016a,b, 2017; Pawlak et al. 2016). The recent *Gaia* Data Release 2 (Gaia Collaboration et al. 2018) contains about 5×10^5 variables (Holl et al. 2018). Additional examples of surveys providing large numbers of new variable stars are the All-Sky Automated Survey (ASAS; Pojmanski 1997, 2002), the All-Sky Automated Survey for Supernovae (ASAS-SN; Shappee et al. 2014; Kochanek et al. 2017; Jayasinghe et al. 2018, 2019b), the Catalina Sky Survey (Drake et al. 2014, 2017), EROS (Kim et al. 2014), MACHO (Alcock et al. 1996, 1997), the Asteroid Terrestrial-impact Last Alert System (ATLAS; Heinze et al. 2018; Tonry et al. 2018), and the Kilodegree Extremely Little Telescope (KELT; Pepper, et al. 2007; Rodriguez et al. 2017).

Spectroscopy can track the motions of a source, whether due to binarity or pulsations, while also providing physical parameters such as the effective temperature, surface gravity, chemical composition, and kinematics. Traditionally, spectra have been obtained as follow-up observations of objects selected from photometric surveys, but stand-alone time-resolved spectroscopy is gradually becoming available due to the advent of large spectroscopic surveys including the Apache Point Observatory Galactic Evolution Experiment (APOGEE; Majewski et al. 2017), the Galactic Archaeology with HERMES (GALAH; De Silva et al. 2015), the Large Sky Area Multi-Object Fiber Spectroscopic Telescope (LAMOST; Zhao et al. 2012), and the Radial Velocity Experiment (RAVE; Steinmetz et al. 2006). This allows the investigation of questions that would be difficult to address with purely photometric data.

In particular, APOGEE used the 2.5-m telescope of the Sloan Digital Sky Survey (SDSS; York et al. 2000) to obtain high-resolution ($R = 22\,500$), high signal-to-noise ratio (S/N > 100), infrared spectra for about 3×10^5 stars with the goal of estimating radial velocities to a precision of $200\,\mathrm{m\,s^{-1}}$ along with the elemental abundances for 20 chemical species to a precision 0.1 dex (García Pérez et al. 2016; Majewski et al. 2017). Because of the APOGEE target selection strategy, the observed sample consists mostly of red giants (Zasowski et al. 2013). Many of the targets were observed on multiple (up to a few tens) visits, which makes this sample a gold mine for studying variable and binary stars.

Several authors have searched the APOGEE data for binary stars. Badenes et al. (2018) used the distributions of maximum radial velocity shifts among multiple APOGEE visits as a proxy for stellar multiplicity, finding that low-metallicity stars have higher radial velocity shifts and hence a higher multiplicity fraction than metal-rich stars. This has many implications for star formation, evolution, and demise, including for the progenitors of gravitational wave sources. Moe, Kratter & Badenes (2019) also found a strong metallicity dependence in a joint analysis of heterogeneous samples of binaries, including APOGEE. El-Badry et al. (2018) fit APOGEE spectra as a superposition of multiple model spectra, leaving aside the radial velocity information, and identified ~ 2700 candidate main-sequence multiple stars. Radial velocities of about ~ 700 of these stars of these were found to be variable but with no trace of a secondary in the spectrum. Full orbital solutions were obtained for 64 systems, and mass ratios were estimated for ~ 600 binaries from multi-epoch radial velocities. Finally, Price-Whelan et al. (2018) used a custom-built Monte Carlo sampler to find periods and other orbital parameters from radial velocity measurements of red giants in APOGEE. They found 320 systems with confident estimates of the orbital parameters, and ~ 5000 stars likely to be binaries. Price-Whelan & Goodman (2018) then used this sample to examine tidal circularization theory.

Clearly, the small number of epochs presents an obstacle to characterizing the orbital properties of binaries in spectroscopic time-domain surveys: the likelihood space for the period is vast with many peaks (Price-Whelan et al. 2018). However, periods can be reliably and precisely determined from photometry if the binary system is eclipsing or displays detectable ellipsoidal or rotational variability. Thompson et al. (2018) obtained photometric periods from the All-Sky Automated Survey for Supernovae (ASAS-SN; Shappee et al. 2014) for several hundred APOGEE targets with the largest radial velocity accelerations. This led to the identification of a binary with an unseen $2.5–5.8\,\mathrm{M_\odot}$ companion, a first likely non-interacting binary star composed of a black hole with a field red giant with implications for physics of supernovae, black holes, and binaries (Breivik, Chatterjee & Andrews 2019).

This illustrates the great synergy in the study of binary stars that can be realized by combining spectroscopic and photometric surveys and we expect similar gains for other types of variable stars. The amount of time-resolved spectroscopic data will increase rapidly in the future. For example, the Milky Way Mapper project in SDSS-V survey plans to obtain spectra of more than 4 million stars at multiple epochs, starting in 2020 (Kollmeier et al. 2017). Simultaneously, many efforts in the field of photometric time-domain surveys will culminate with the Large Synoptic Survey Telescope scheduled to commence scientific operations in 2023 (LSST Science Collaboration et al. 2009).

In this paper, we perform a detailed search and classification of periodic variable stars among APOGEE targets using photometric data from the ASAS-SN survey (Shappee et al. 2014). This paper is intended as a catalogue, with more detailed investigations of individual variable classes deferred to further papers. The structure of the paper is as follows: Section 2 describes the ASAS-SN and APOGEE data; Section 3 presents the procedure used to select and classify the variable stars and the catalogue itself; Section 4 discusses the results including a comparison to previously identified binaries in APOGEE; and Section 5 summarizes the results.

2 DATA

We start with the APOGEE Data Release 14 (DR14; Abolfathi et al. 2018) and obtain light curves for the 258 484 targets from ASAS-SN. ASAS-SN (Shappee et al. 2014) is a photometric transient survey covering the whole sky. The observations used in this study were carried out with the original two quadruple telescope units (Brutus at Haleakala, Hawaii, and Cassius at CTIO, Chile) and have a limiting magnitude of $V \sim 17$ mag. ASAS-SN went through an expansion at the end of 2017, adding three new g-band units and has recently switched Brutus and Cassius to g-band as well. The g-band limiting magnitude is ~ 18, and these observations will be used in future studies. The field of view of each camera is 4.5 deg^2, the pixel scale is 8 arcsec, and the full width at half-maximum is ~ 2 pixels. The ASAS-SN photometry is obtained with differential image analysis (Alard & Lupton 1998; Alard 2000), with aperture photometry on the subtracted frames. Details of the procedure are described in Jayasinghe et al. (2019b). Further technical details of the ASAS-SN survey were described by Kochanek et al. (2017). ASAS-SN recently published a sample of over 66 000 serendipitously discovered variable stars (Jayasinghe et al. 2018), reclassified over 4×10^5 known variable stars (Jayasinghe et al. 2019b) from the Variable Stars Index (VSX; Watson, Henden & Price 2006), and identified 11 700 variables in the southern *Transiting Exoplanet Survey Satellite* continuous viewing zone (Jayasinghe et al. 2019a).
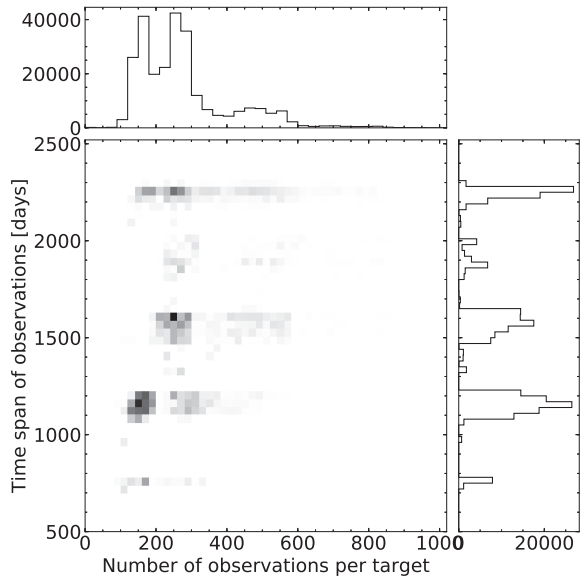
Figure 1. Number of data and time span of observations of the APOGEE DR14 targets from the ASAS-SN survey.
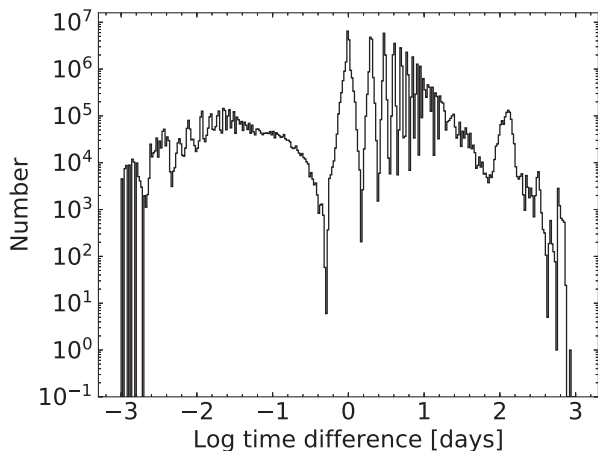

Figure 2. Time-sampling properties of ASAS-SN shown as a histogram of the time differences between two consecutive observations of the same object, for all objects. The histogram uses bins equally spaced in the logarithm of the time difference.

In Fig. 1, we show the the total number of photometric observations and the time span of the data for all our light curves. The majority of the targets were observed for more than 3 yr and typically have at least 150 measurements. The median number of photometric measurements is 248, but there are objects with 600 or more measurements. The structure in Fig. 1 is due to the history of how Cassius and Brutus were built and filled with telescopes (see Kochanek et al. 2017).

Since ASAS-SN operates several telescopes at different sites, we also investigate the cadence and time-sampling properties. In Fig. 2, we show the distribution of time differences between two consecutive measurements. There are observations separated by ≪1 d, which is caused by overlap between the fields of view of the telescopes in each unit. Peaks at integer numbers of days are due to diurnal observations from one site, and a small bump at ∼100 d corresponds to the typical seasonal gap. Further details on

photometric properties of ASAS-SN, including characterization of the time sampling and the window function in frequency space, were presented by Jayasinghe et al. (2018, 2019b).

3 VARIABILITY CLASSIFICATION

3.1 Period search

The first step in the process of identifying periodic variable stars is a period search. We searched all of the light curves in the sample for periodicity using two independent methods. The first is the Lomb–Scargle periodogram method (LS; Lomb 1976; Scargle 1982) based on the Fourier transformation. This approach is especially useful for sinusoidal variability and for light curves that are well represented by a low-order Fourier sequence (e.g. pulsating stars). However, the LS method often fails to find periods for variables with strongly non-sinusoidal light curves such as those of detached eclipsing binaries. In order to identify the correct periods for the eclipsing binaries, we used the Box Least Square (BLS) method (Kovács, Zucker & Mazeh 2002). The BLS algorithm was designed to look for planetary transits, making it better suited for detecting eclipsing variability.

We used the implementations of both period search algorithms in the VARTOOLS package (Hartman & Bakos 2016). We selected the candidates for periodic variables based on the S/N of both methods. We set the threshold to S/N > 30 for the LS method and to S/N > 350 for the BLS method. Objects satisfying at least one of these criteria were identified as candidates.

3.2 Visual inspection

We visually inspected all of the selected candidates. The variables were divided into the following classes: eclipsing and ellipsoidal binaries, classical pulsators, rotational variables, long-period variables (LPV), including Miras and long secondary period variables (LSP). The binary stars are further subdivided into detached (EA), semidetached (EB), contact (EW), and ellipsoidal (ELL) systems. EW systems have a smooth transition from the eclipse to the out-of-eclipse phase, and two minima of equal or very similar depth. EB stars also have smooth light curves, however the depth of the eclipses can be significantly different. EA systems have light curves that allow the determination of the beginning and end of the eclipse. ELL binaries do not show eclipses because of the orbital inclination, but they can still be identified as binaries due to the tidal deformation of a star in the system.

Classical pulsators are stars that occupy the main instability stripe in the Hertzsprung–Russell diagram. They are divided into δ Scuti stars with periods shorter than 0.2 d, RR Lyrae stars with $0.2 < P < 1.0$ d, and Classical and Type II Cepheids with the typical periods longer than 1 d.

LPV stars are pulsating red giants, with typical periods from 20 to a few hundred days. The majority of these objects are relatively small-amplitude pulsators belonging to the semiregular variable (SRV) or OGLE Small-Amplitude Red Giants (OSARG; Wray, Eyer & Paczyński 2004) classes. The much less abundant Miras are easily distinguishable by their high amplitudes, reaching a few magnitudes. Finally, there is a group of LPVs showing the Long Secondary Period (LSP) phenomenon: additional variability, on much longer periods and higher amplitudes. The origin of LSPs remains unclear (e.g. Wood, Olivier & Kawaler 2004). For LSPs we report the longer period as the main period of the variability.

The last of the variability classes consists of the rotational variables. These objects are mostly different types of spotted stars. They can show a broad spectrum of light curve morphologies and are usually the most difficult to precisely classify. Most of the stars that show periodic variability, but do not fit into the pulsating or binary classes, are classified as rotational. However, some rotational variables might be close binaries with inclinations not allowing us to see the eclipses. The total number of likely periodic variables detected in this step is 1980.

3.3 Machine learning

In order to verify the visual classification, we employed the Random Forest machine learning classification pipeline built from the previous ASAS-SN variability studies (Jayasinghe et al. 2018, 2019b). The classification is done using 17 features, including infrared colours from the Two Micron All Sky Survey (2MASS; Skrutskie et al. 2006), extinction-corrected absolute magnitudes based on *Gaia* DR2 (Bailer-Jones et al. 2018; Gaia Collaboration et al. 2018), as well as various statistical parameters and Fourier parametrizations of the light curve. A detailed description of the latest version of the classifier is presented in Jayasinghe et al. (2019b).

All objects identified in the previous step were passed through the classifier. For 1342 objects, the machine learning classification was consistent with the previously attributed class, and for 572 it was different. We re-inspected the discrepant cases visually. The classification of 393 objects was changed to the one given by the machine learning classifier, while for 179 objects the original classification was retained. The total number of instances correctly classified by the Random Forest classifier is 1735. This gives us an estimate for the classifier accuracy of about 91 per cent. In addition 66 objects were removed from the final sample during re-inspection as being too noisy and 10 objects, which were identified while working on another APOGEE related project, were added.

3.4 Damped random walk

The APOGEE target selection function includes a large fraction of red giants, which often exhibit semiregular or even completely irregular variations. In order to characterize this variability and to compare with the periodic classification, we also modelled the light curves using the Damped Random Walk (DRW) stochastic process. The DRW is defined by the covariance function

$$S_{ij} = \sigma \exp(-\left|t_i - t_j\right|/\tau) \tag{1}$$

between times t_i and t_j, where σ describes the variance of the light curve on long time-scales and τ is the coherence time. After removing objects with too few measurements (<30) and substituting missing values of photometric uncertainties with the mean of uncertainties from the rest of the data points for that particular object, we fitted 248 867 light curves using the Gaussian processes module CELERITE (Foreman-Mackey et al. 2017). An additional linear parameter $\overline{m}$ was introduced to remove the light-curve mean. To allow for photometric uncertainties we add a noise matrix to the process covariance matrix S_{ij}. The best-fitting parameters σ and τ were obtained by maximizing the log-likelihood function using a SCIPY implementation of the Broyden–Fletcher–Goldfarb–Shanno (BFGS) optimization routine (Broyden 1969), with bounds 0.1 and 1000 d on the parameter τ and no bounds on σ and $\overline{m}$. The initial values were chosen at random from a uniform distribution for τ, set

Table 1. Number of variables by class.

Type	Subtype	Number
ECL		430
	EA	203
	EB	126
	EW	65
	ELL	36
Pulsating		139
	δ Scuti	11
	RR Lyrae	108
	Class Cepheids	15
	Type II Cepheids	6
LPV		719
	Mira	10
	LSP	185
	SRV/OSARG	524
Rotational		636
Total		1924

to the standard deviation of the observed magnitudes for σ, and to the light-curve mean for $\overline{m}$.

We used the variances of these parameters as a proxy for the goodness of fit, leveraging the fact that the inverse Hessian matrix of the log-likelihood function provides a reasonable estimate of the variance–covariance matrix of parameters at the maximum, as shown in appendix A of Yuen (2010). Models with variance greater than one (in log-scale) in either parameter were discarded, as were those with decorrelation time τ comparable to the survey duration ($\gtrsim 1000$ d). Because of the survey duration, we can only reasonably identify objects with $\tau \lesssim 100$ d (see Kozłowski 2017).

3.5 Catalogue

The final sample consists of 1924 periodic variables. This includes 430 binary stars, 719 LPV, including 185 LSP variables, 139 classical pulsators, and 636 rotational variables. A summary of the catalogue is presented in Table 1. For each of the objects with a *V*-band ASAS-SN light curve, we give the position on the sky, the period, the variability classification, and the APOGEE DR14 spectroscopic parameters (surface gravity log g, rotational broadening $v\sin i$, effective temperature $T_{\rm eff}$, and metallicity [Fe/H]). The data are available via the ASAS-SN data repository at https://asas-sn.osu.edu/variables. Additionally, we provide the ASAS-SN photometry for all of the APOGEE targets at https://asas-sn.osu.edu/photometry.

We also cross-matched the sample with the variable star catalogues of OGLE, *Gaia* DR2, MACHO, ATLAS, and KELT surveys, as well as to the VSX (Watson et al. 2006). Out of the 1924 objects, 1460 were found in these catalogues of variable stars and 464 are likely new discoveries. Our classification was consistent with the literature for 703 and different for 757 known variables. Figs 3–7 show example light curves of the objects from the catalog.

4 DISCUSSION

Here we discuss the overall characteristics of the variability in the APOGEE targets using both the photometric and spectroscopic information. We plan to perform a more detailed analysis for individual classes of variable stars in future papers. Specifically, we outline interesting differences between LSP stars and other LPVs, which will be investigated in a following paper.

4.1 APOGEE parameters

We use the spectroscopic parameters taken from ASPCAP (García Pérez et al. 2016). In Fig. 8, we present the cumulative distributions in $\log g$ for the whole APOGEE sample and for individual classes of variables. The APOGEE sample consists of a mixture of giants ($\log g < 1.0$), dwarfs ($\log g > 2.0$), and subgiants ($1.0 < \log g < 2.0$).

The distribution of all variables (black dashed line) follows this trend, but with a higher variability fraction for red giants (LPV and LSP). Rotational variables (green line) are found mostly on the main sequence, while the eclipsing and ellipsoidal variables are also detected among the red giants. Classical pulstors are not shown in Fig. 8 and the later figures, since the number of these objects with APOGEE parameters is too small to analyse their distribution.

We show the cumulative distributions of effective temperatures ($T_{\rm eff}$) in Fig. 9. Here, we also split the whole APOGEE sample into low and high $\log g$ subsamples, which are separated rather arbitrarily at $\log g = 2$. As can be seen in Fig. 8, more than 90 per cent of LPV have $\log g$ below this value and more than 90 per cent of eclipsing binaries have $\log g > 2$. In this way, we distinguish between dwarfs and giants (grey dashed and dotted lines). We see that the distribution of binary stars is similar to the whole APOGEE sample except that there are more binaries at higher $T_{\rm eff}$. Rotational variables are shifted to lower $T_{\rm eff}$ relative to APOGEE dwarfs, which can be understood as a trend of increasing stellar activity with decreasing $T_{\rm eff}$ (West et al. 2004). As expected, LPV and LSP stars are very cool and have very similar $T_{\rm eff}$ distributions.

In Fig. 10, we show the cumulative distributions in [Fe/H]. We see that the median [Fe/H] of the APOGEE giants is about 0.1 dex lower than for the dwarfs. The rotational variables follow the general trend of the dwarfs, but their distribution is somewhat more compact. The median metallicities for the eclipsing binaries and ellipsoidal variables are shifted by about 0.2 dex to lower [Fe/H] as compared with the dwarfs or the APOGEE catalogue as a whole. Badenes et al. (2018) and Moe et al. (2019) previously noted the higher binary fraction at lower metallicities, but our result is based on a completely different selection method. The distributions of eclipsing and ellipsoidal variables in $\log g$ and $T_{\rm eff}$ are broadly consistent with those of the dwarfs rather than giants due to two effects. First, the binary fraction of red giants should be lower as a result of stellar evolution. Second, it is harder to see the eclipses in main sequence plus giant star binaries. The median [Fe/H] of the LPV and LSP stars is shifted to lower metallicities by 0.3 and 0.5 dex, respectively, relative to the rest of the APOGEE giants. The significant difference between the LPV and LSP will be the subject of a future paper. The median metallicity of the overall sample of variables is about 0.3 dex lower than for APOGEE as a whole.

Finally, Fig. 11 shows the distributions in $v \sin i$. Most of the APOGEE stars have low rotational velocities, $v \sin i \lesssim 15$ km s^{-1}. As expected, $v \sin i$ is significantly higher for rotational variables and even higher for eclipsing and ellipsoidal stars. It can also be seen that about half of the binary sample lies at the upper limit of $v \sin i \approx 90$ km s^{-1}. This is due to the upper limit on $v \sin i$ in ASPCAP. Rotational velocities are unavailable for most of the LPV stars in our sample because the library of giant spectra used in ASPCAP does not include rotation.

4.2 Combining spectroscopic and photometric information

The combination of the ASAS-SN and APOGEE data allows for a more detailed analysis of the sample and verification of the

accuracy of the photometric classifications. In Fig. 12, we present the distribution of the sample in the $\log g$–P plane. The first thing to notice is the clear separation between the red giants, occupying the upper right-hand corner of the plot with long P and low $\log g$, and the rest of the sample. Among the giants, the LPVs with longer P typically have lower $\log g$, which is a manifestation of the dependence of the pulsational period on the mean stellar density. LSPs do not show a similar correlation, partly because they span a relatively smaller period range than LPVs. Even though the LSPs are considered part of the LPV class, for the purpose of this analysis they are treated as a separate group since their secondary period (which is the most prominent source of variability of these objects) is much longer than the typical pulsation periods of LPV stars and likely has a different physical origin.

In Fig. 13, we show the distribution of P with respect to $T_{\rm eff}$. Most of the objects are cool stars with $T_{\rm eff} < 5000$ K, as expected given the APOGEE target selection. However, there are also hotter objects, including Cepheids and some binaries. We do not see any prominent correlations between these parameters. Next, in Fig. 14, we show the distribution in [Fe/H] and P. There is a wide span of metallicities, as expected from the variety of populations targeted by APOGEE. For example, at low [Fe/H], we can identify RR Lyrae stars, while the Cepheids cluster near solar metallicity.

Finally, in Fig. 15, we show the distribution of the sources in the sample in the $v \sin i$ –P plane. We see a broad sequence with $v \sin i$ decreasing with period. This sequence is mostly formed by rotational variables and eclipsing binaries, where such a relation is expected. The clumping of stars around 90 km s^{-1} is again due to the upper limit on $v \sin i$ in ASCAP.

4.3 DRW results

There have not been many works applying stochastic or quasi-periodic models to photometry of variable stars (see Kozłowski et al. 2010; Zinn et al. 2017, and the references therein). It is therefore worthwhile to investigate DRW models of the APOGEE variable stars. In Fig. 16, we show the distribution of all 47 828 objects with well-fitted light curves (defined as an uncertainties in $\ln \sigma$ and $\ln \tau$ smaller than unity and $\sigma \geq 0.001$) with a two-dimensional histogram shown as grey bitmap. The concentration of objects at τ of few days (the typical cadence of the survey, Fig. 2) is likely caused by the noise being higher than what is reported in photometric uncertainties. As the DRW time-scale becomes shorter than the observing cadence, the model increasingly resembles white noise (i.e. uncorrelated photometric errors). Indeed, if we apply even a mild a cut of σ greater than twice the median photometric uncertainty, the number of objects drops to 17 530.

Objects classified as periodic variables are shown with coloured points in Fig. 16. These objects have $\sigma \gtrsim 0.02$ mag and occupy distinct regions. For example, DRW typically picks up the shorter pulsational period of the LSPs, so they occupy a nearly identical parameter region to the LPVs. The correlation between σ and τ for these objects is expected from pulsational models of red giants, where the pulsational period and growth rate of modes increase with the radius of the star (Trabucchi et al. 2019).

It is also of interest to compare the DRW variability time-scale τ with the periods from Section 3.1. Fitting the DRW models is comparable in terms of computational effort to Fourier analysis, but it is faster than a BLS search, which is especially useful for detached binaries. In Fig. 17, we compare P and τ for our sample of variable stars. We see that there is a clear correlation between these two quantities and for different types variable stars. However,
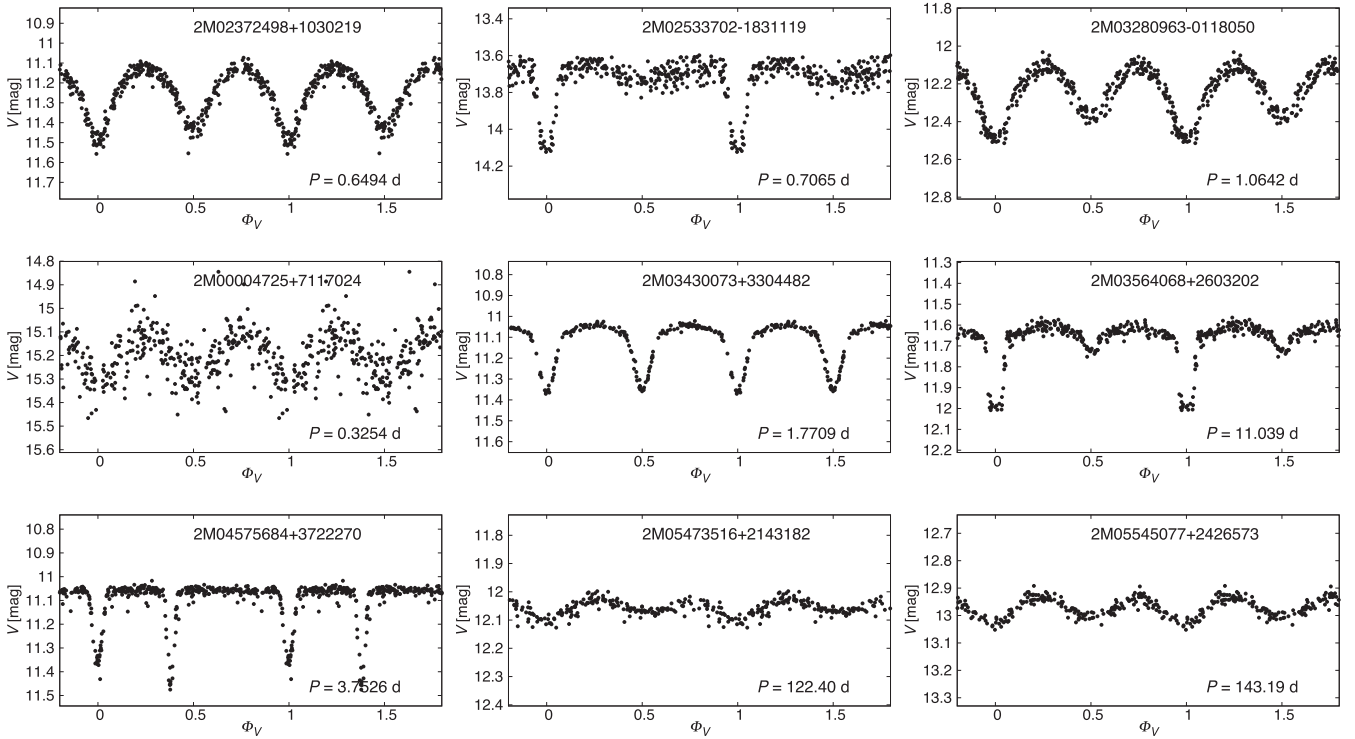
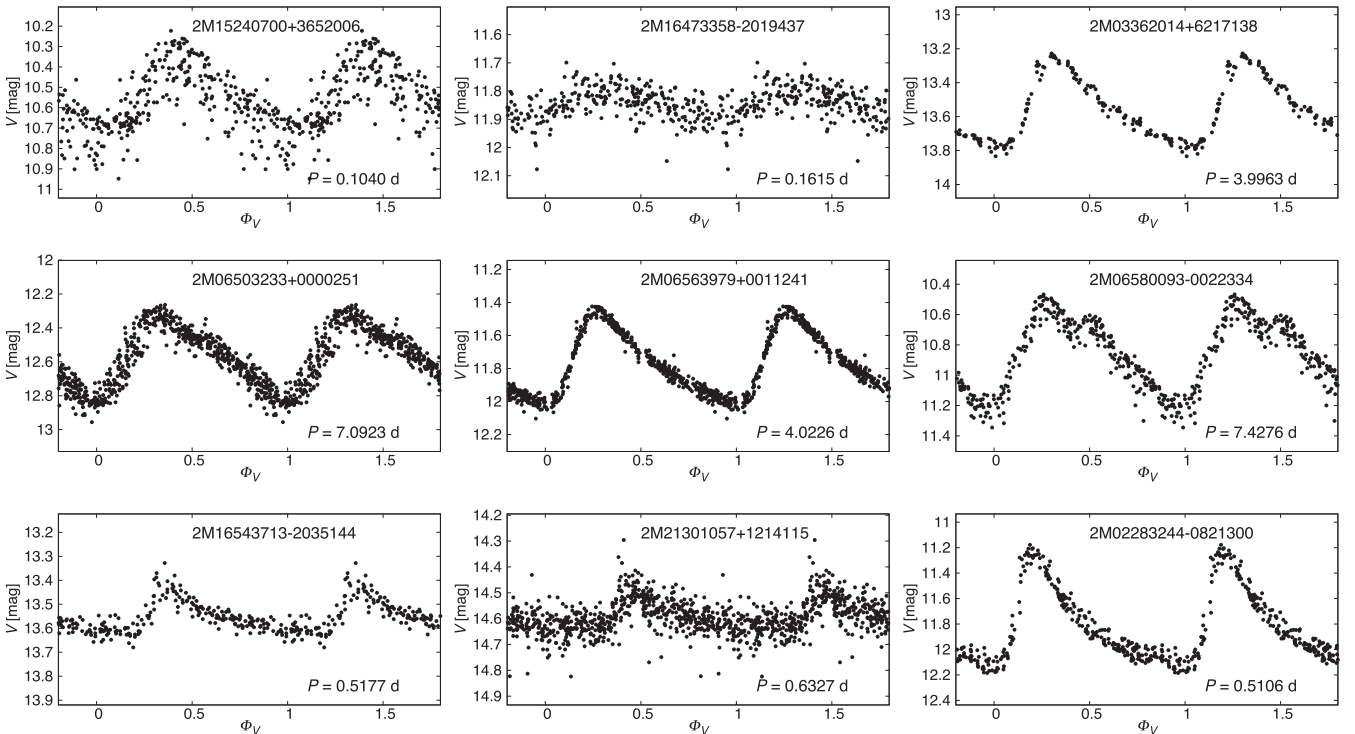**Figure 3.** Example light curves of binary stars from the catalogue.

Figure 4. Example light curves of pulsating variables from the catalogue.

the correlation is very weak for eclipsing binaries, where sharper features like occultation ingress and egress dominate the DRW inferences. Interestingly, the relation between P and τ is not linear, but power law with an exponent of approximately 0.6 (Kozłowski et al. 2010; Zinn et al. 2017). Fig. 17 also illustrates the expected fact that DRW cannot reliably infer variability time-scales shorter than the survey cadence: for $P \lesssim 3$ d, the correlation between P and τ breaks down. This limits the utility of DRW for classifying
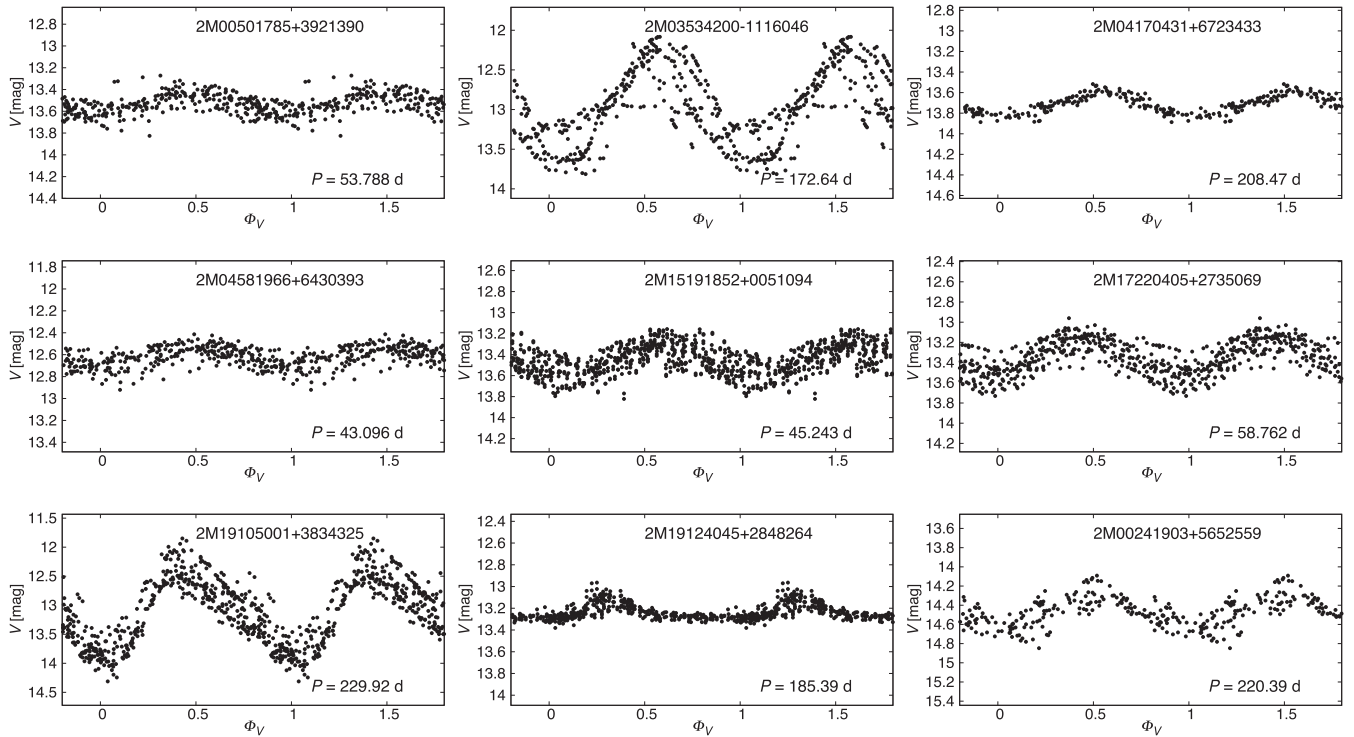
Figure 5. Example light curves of LPV variables from the catalogue.
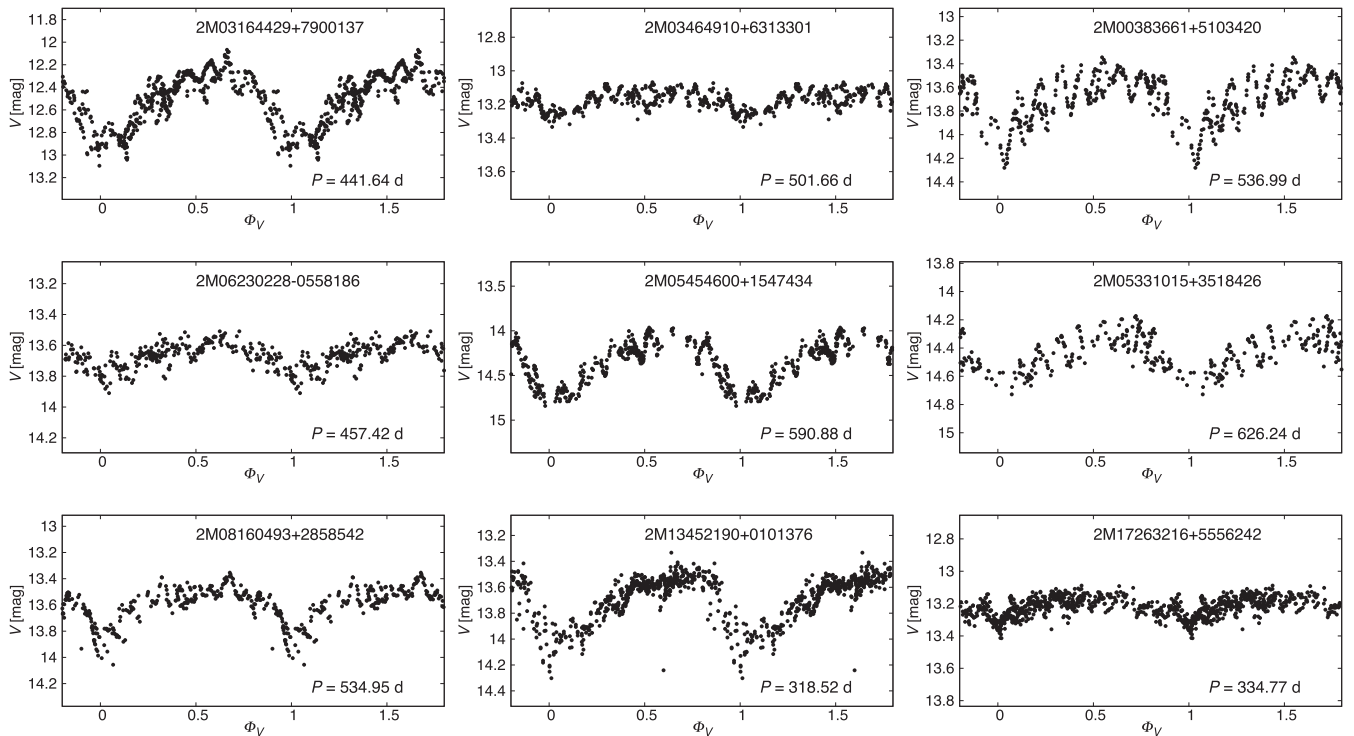
Figure 6. Example light curves of LSP variables from the catalogue.

variability in surveys with long cadence. The upper limit on $\tau \lesssim 100$ d is defined by the survey duration ($\sim$1000 d). The majority of the objects in our sample have τ in the region where it can be reliably recovered, but values τ at both the lower and higher end of the distribution should be interpreted with caution.

4.4 Comparison with previous searches for binary stars in APOGEE

Comparing our sample of 1924 variable stars with spectroscopic searches based on radial velocities or spectral fitting allows us to assess the completeness of both approaches. We first cross-matched
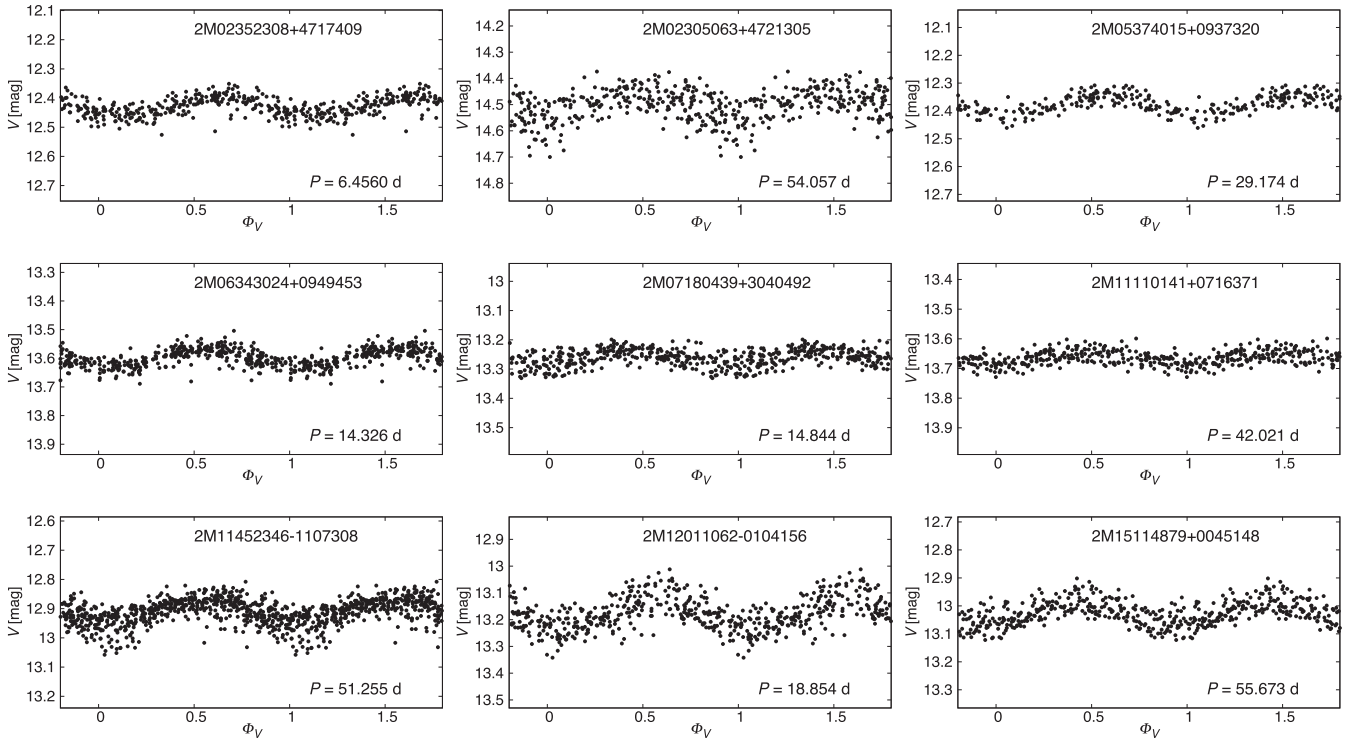
Figure 7. Example light curves of rotational variables from the catalogue.
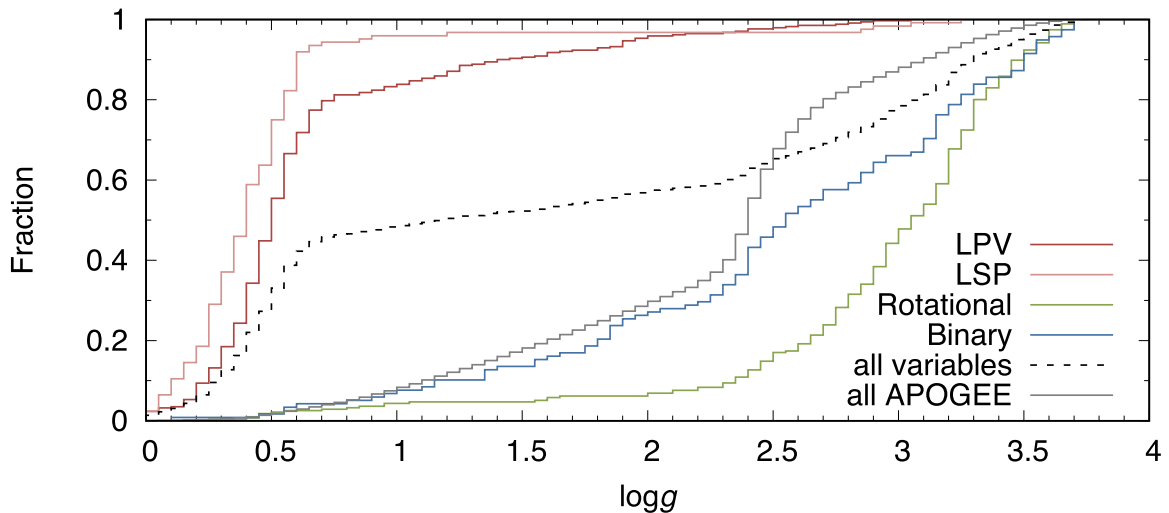
Figure 8. Cumulative distribution of log g for variable objects and the APOGEE catalogue as whole.

our sample with the list of spectroscopic binaries from El-Badry et al. (2018). This catalogue consists of 20 141 dwarfs, 16 833 of them classified as spectroscopically single, 663 as SB1, 2423 as SB2, 108 as SB2 with an underlying third body signal, and 114 as SB3. We found that 171 of our variable sources are also in the El-Badry et al. (2018) catalogue, with 70 classified as single stars and 101 identified as binary or triple systems. Out of the 70 stars classified as spectroscopically single by El-Badry et al. (2018), 32 were identified in our sample as eclipsing binaries. The remaining 38 objects were classified as rotational variables (35 objects) or pulsating stars (3 objects).

Out of 101 stars that were identified as binary or triple by El-Badry et al. (2018), 42 were also classified as eclipsing in

our list, with 19, 20, 2, and 1 classified as SB1, SB2, SB2 with underlying third body signal, and SB3, respectively. The remaining 59 spectroscopic binary candidates from El-Badry et al. (2018) were classified as rotational (58 objects) or pulsating (1 object) variables in our catalogue.

We also matched to the list of binaries identified based on radial velocity variations from Price-Whelan et al. (2018), who classified 320 objects as uniquely determined binaries (having unimodal posterior for the period) and 106 as binaries with bimodal period posteriors, among the 96 231 APOGEE targets that were analysed. Only seven systems (1.6 per cent of our list) overlap with our catalogue. Four of them were flagged as uniquely determined binaries and three as binaries with bimodal sampling.
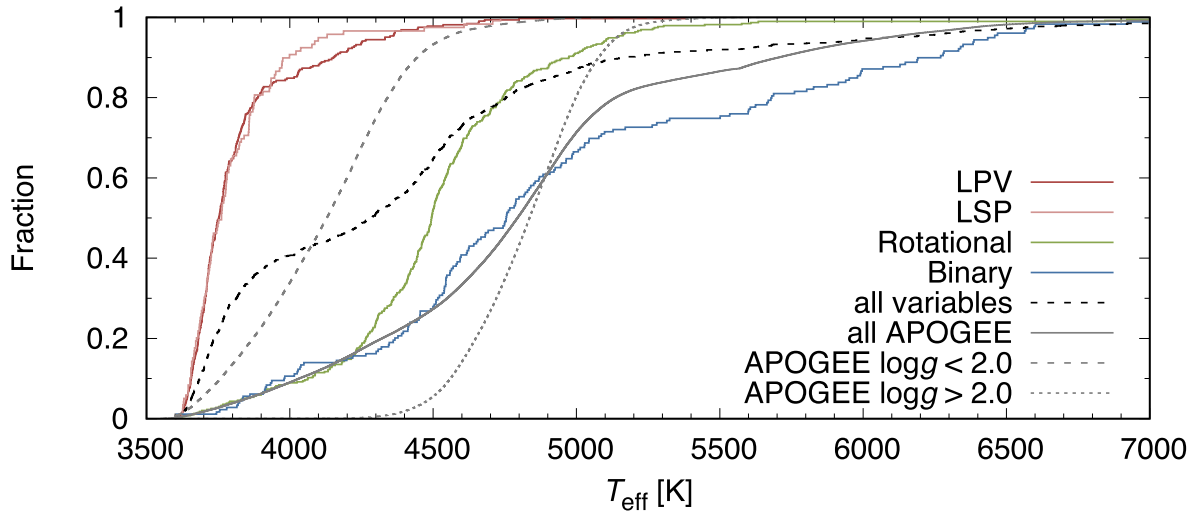
Figure 9. Same as Fig. 8, but for T_{eff}.
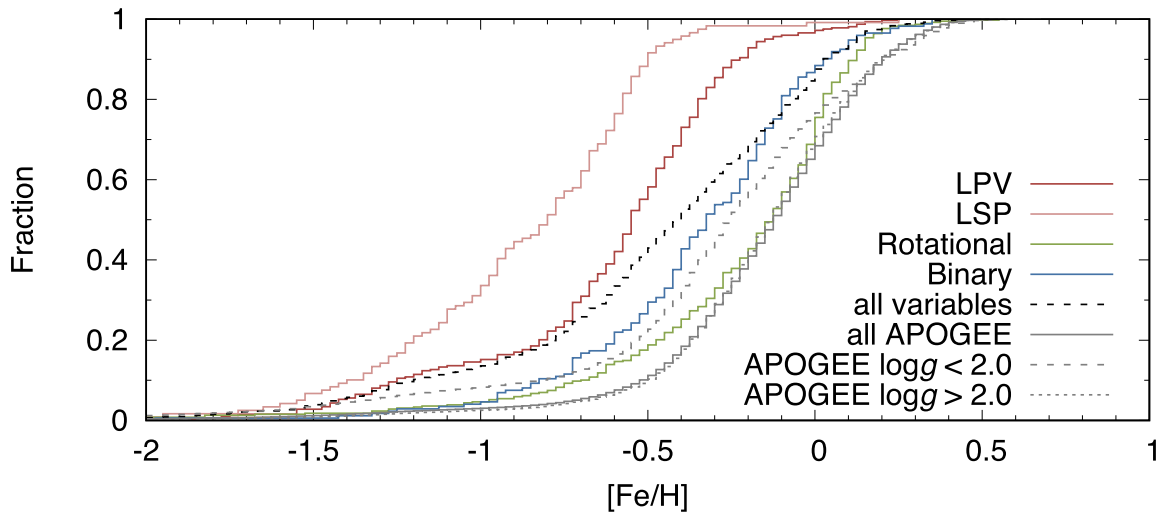
Figure 10. Same as Fig. 8, but for [Fe/H].
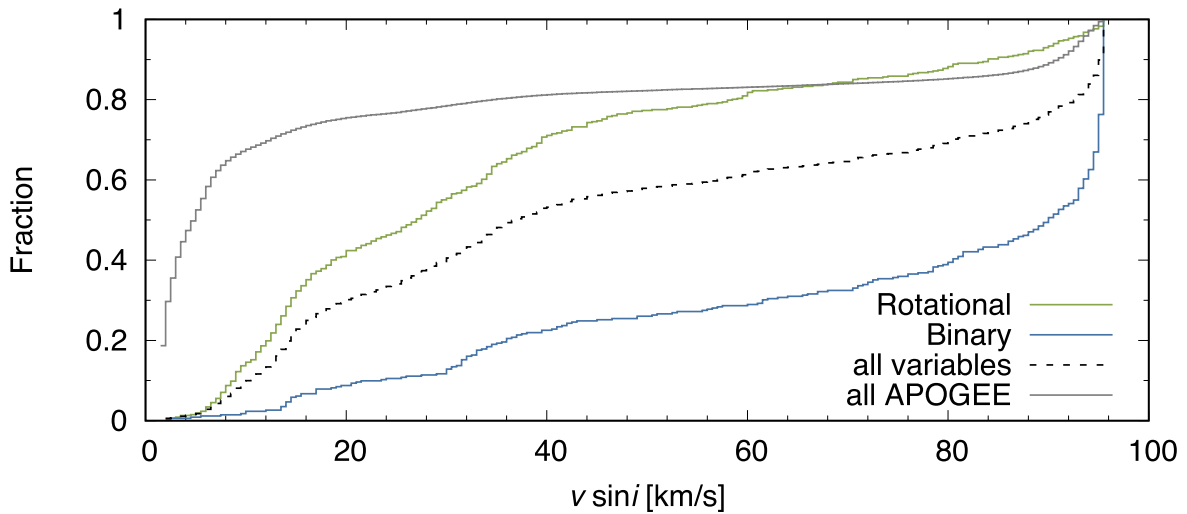
Figure 11. Same as Fig. 8, but for $v\sin i$.
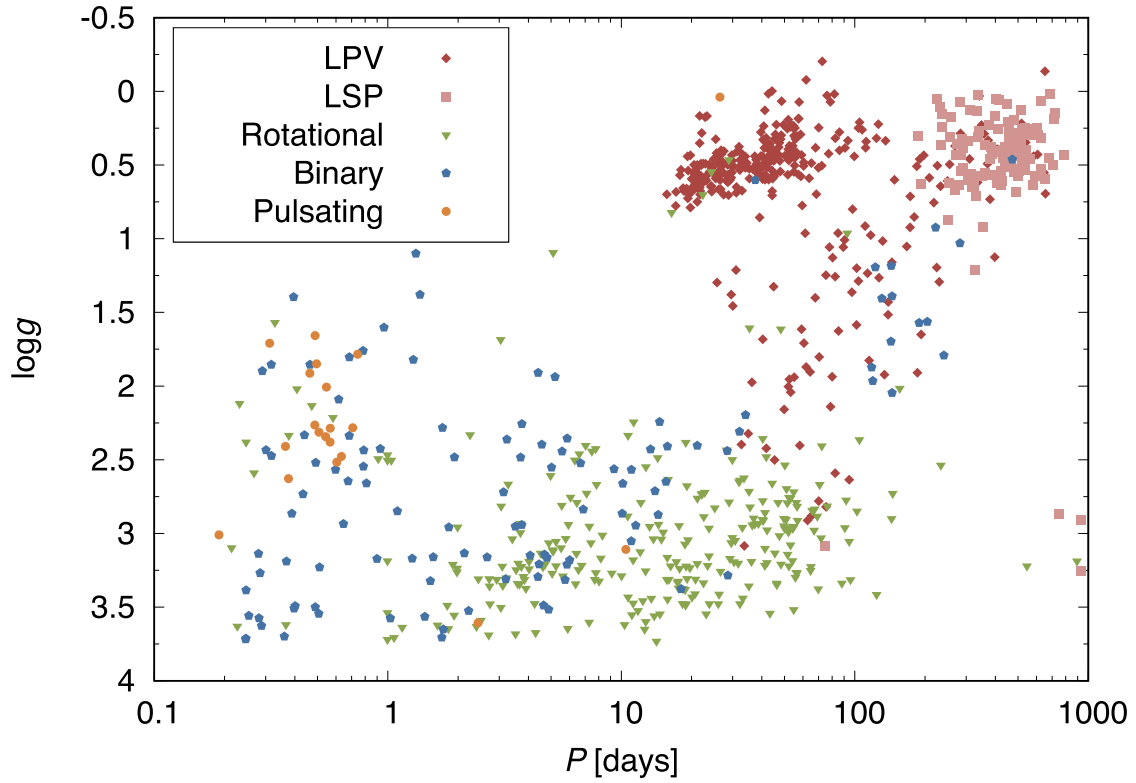
Figure 12. Variable stars in the P–$\log g$ plane. LPV stars are marked with red, LSP with pink, binary stars with blue, rotational variables with green, and classical pulsators with orange points.
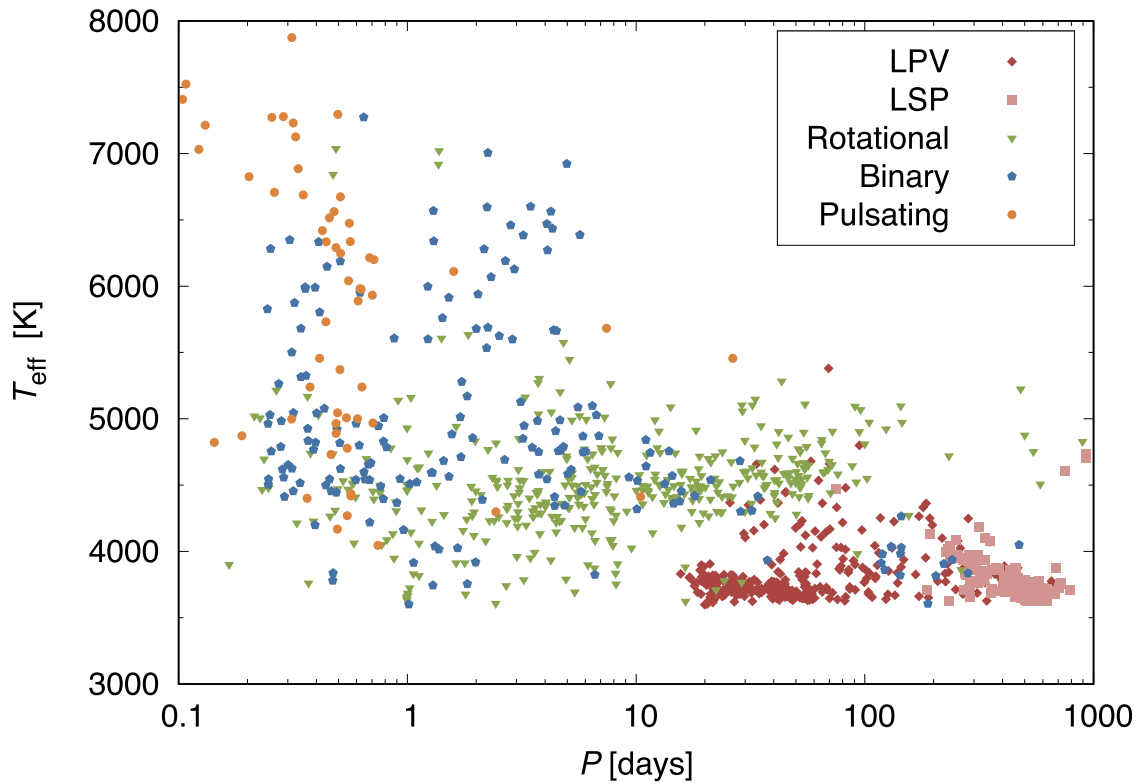
Figure 13. Variables in the $P - T_{\text{eff}}$ plane. The meaning of colours is the same as in Fig. 12.
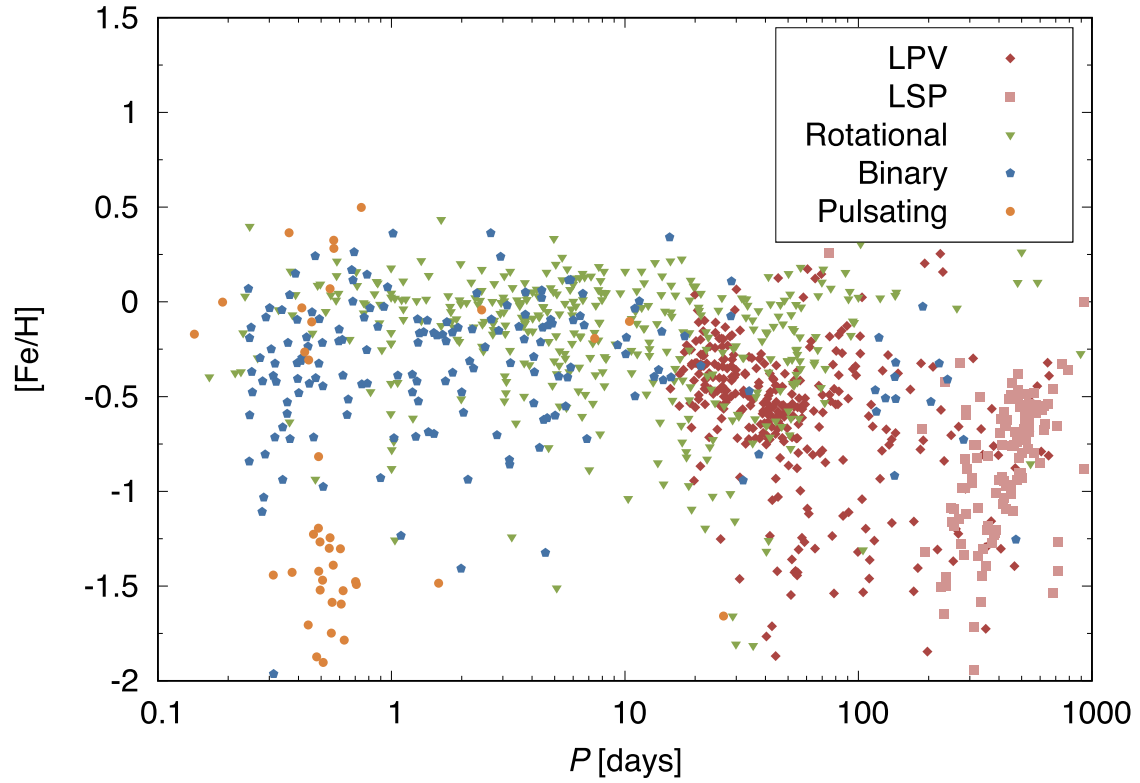
Figure 14. Variables in the *P*–[Fe/H] plane. The meaning of colours is the same as in Fig. 12.
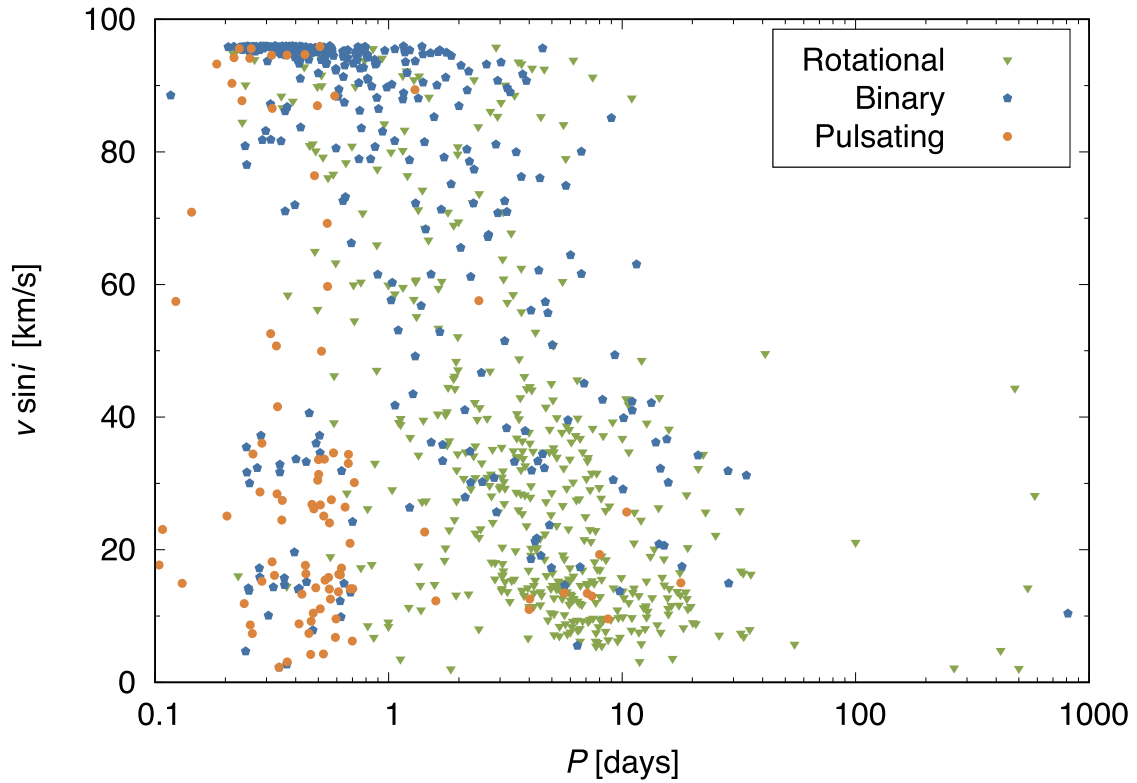
Figure 15. Variables in the *P*–*v*sin *i* plane. The meaning of colours is the same as in Fig. 12.
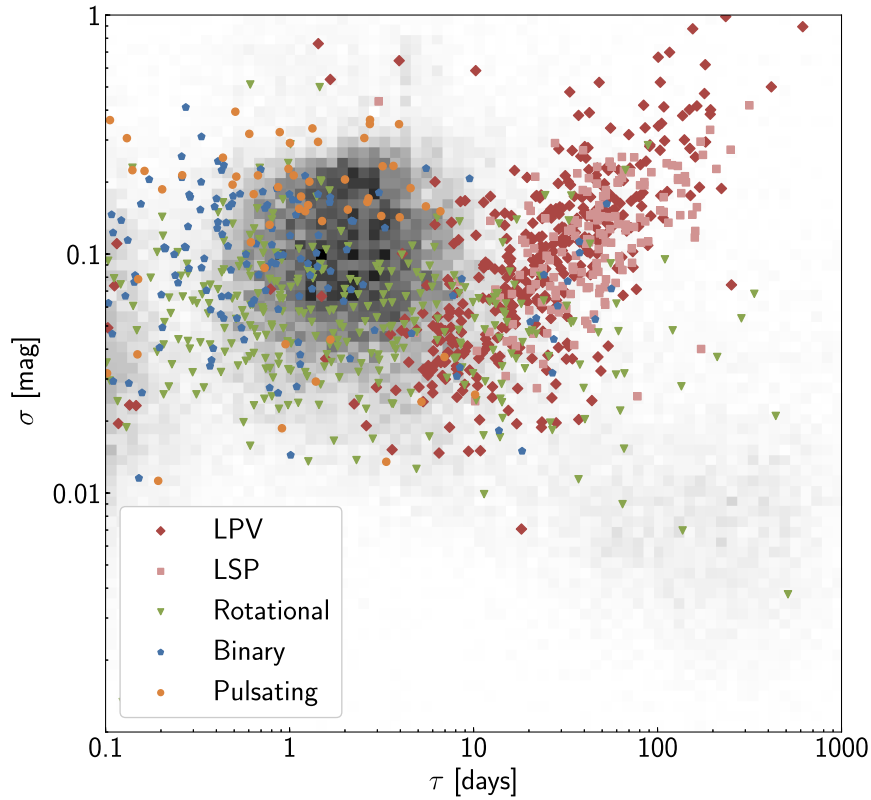
Figure 16. Amplitude of the variability σ relative to the decorrelation time-scale τ for the DRW models. Grey pixels in the background encode the density of all well-fitted light curves. The coloured points denote objects classified as variable, and the meaning of colours is given in the legend.
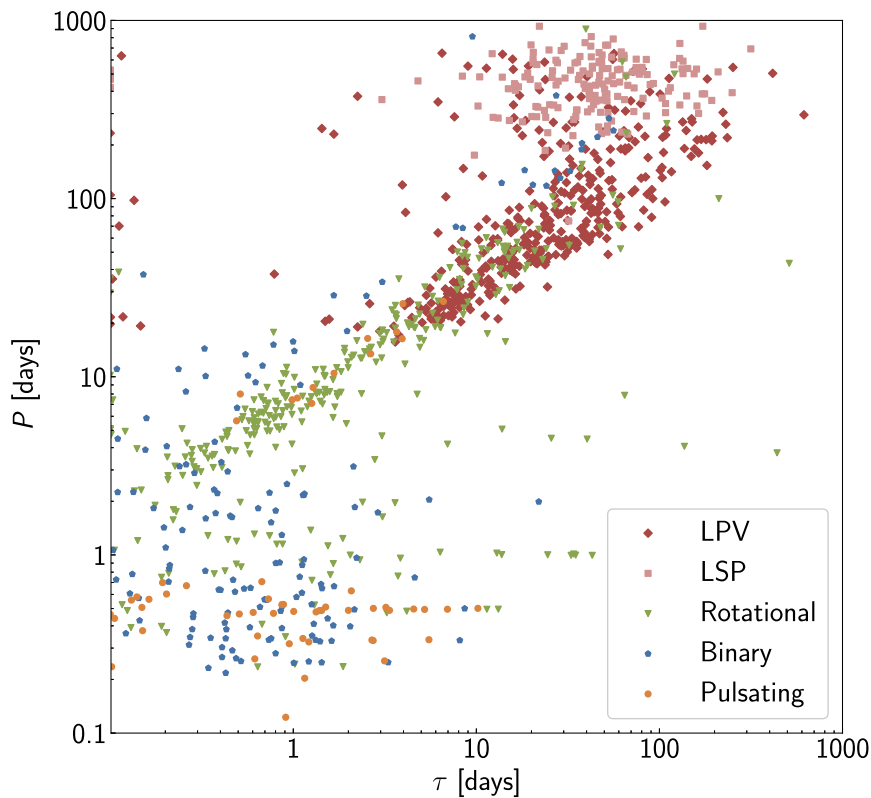
Figure 17. Comparison of the photometric period P with the DRW decorrelation time τ.

The periods of the uniquely determined binaries from Price-Whelan et al. (2018) are in good agreement with the photometricaly derived ones. The fractional difference is <2 per cent for all four systems, and for two, the agreement is ∼0.01 per cent. On the other hand, most the periods derived for the bimodal binaries differ significantly from the photometric ones, even though in one case the difference is relatively low (3.5 per cent).

5 SUMMARY

We performed an independent search for periodic variables in the APOGEE survey using light curves from ASAS-SN. The search was done with both visual inspection and machine learning techniques. The light curves were also modelled with the DRW stochastic process, allowing us to compare these approaches. The final classification of every object was verified manually.

The total number of identified periodic variables is 1924, of which 465 are likely newly discovered. The sample include 430 eclipsing and ellipsoidal binaries, 139 classical pulsators, 719 LPVs, and 636 rotational variables. For each of these objects, we make the ASAS-SN photometric data publicly available at: https://asas-sn.osu.edu/variables. The APOGEE spectra and spectroscopically derived parameters, including: $\log g$, $v\sin i$, $T_{\rm eff}$, as well as chemical abundances of 26 elements, are available in the APOGEE DR14. We also make the ASAS-SN photometry of all the APOGEE targets avalaible at https://asas-sn.osu.edu/photometry.

We then compared the distribution of the variable stars and the overall APOGEE sample in $\log g$, $T_{\rm eff}$, [Fe/H], and $v\sin i$. Like Badenes et al. (2018) and Moe et al. (2019), we find an anticorrelation between binarity fraction and metallicity, but using a completely different selection method. In fact, the whole population of variables has a lower average metallicity than the APOGEE target sample as a whole. There is also a strong correlation of binary and rotational variables to high $v\sin i$.

REFERENCES

Abolfathi B. et al., 2018, ApJS, 235, 42
Alard C., 2000, A&AS, 144, 363
Alard C., Lupton R. H., 1998, ApJ, 503, 325
Alcock C. et al., 1996, AJ, 111, 1146
Alcock C. et al., 1997, AJ, 114, 326
Astropy Collaboration et al., 2013, A&A, 558, A33
Badenes C. et al., 2018, ApJ, 854, 147
Bailer-Jones C. A. L., Rybizki J., Fouesneau M., Mantelet G., Andrae R., 2018, AJ, 156, 58
Breivik K., Chatterjee S., Andrews J. J., 2019, ApJ, 878, L4
Broyden C. G., 1969, Not. Am. Math. Soc., 16, 670
Dambis A. K. et al., 2015, Astron. Lett., 41, 489
Deb S., Singh H. P., 2014, MNRAS, 438, 2440
De Silva G. M. et al., 2015, MNRAS, 449, 2604
Drake A. J. et al., 2014, ApJS, 213, 9
Drake A. J. et al., 2017, MNRAS, 469, 3688
El-Badry K. et al., 2018, MNRAS, 476, 528
Foreman-Mackey D., Agol E., Ambikasaran S., Angus R., 2017, AJ, 154, 220
Gaia Collaboration et al., 2018, A&A, 616, A1
García Pérez A. E. et al., 2016, AJ, 151, 144
Graczyk D. et al., 2014, ApJ, 780, 59
Hartman J. D., Bakos G. Á., 2016, Astron. Comput., 17, 1
Haschke R., Grebel E. K., Duffau S., 2012, AJ, 144, 106

Heinze A. N. et al., 2018, AJ, 156, 241
Hełminiak K. G. et al., 2015, MNRAS, 448, 1945
Holl B. et al., 2018, A&A, 618, A30
Jacyszyn-Dobrzeniecka A. M. et al., 2017, Acta Astron., 67, 1
Jayasinghe T. et al., 2018, MNRAS, 477, 3145
Jayasinghe T. et al., 2019a, MNRAS, 485, 961
Jayasinghe T. et al., 2019b, MNRAS, 486, 1907
Jones E. et al., 2001, SciPy: Open Source Scientific Tools for Python
    (http://www.scipy.org)
Kim D.-W., Protopapas P., Bailer-Jones C. A. L., Byun Y.-I., Chang S.-W.,
    Marquette J.-B., Shin M.-S., 2014, A&A, 566, A43
Kochanek C. S. et al., 2017, PASP, 129, 104502
Kollmeier J. A. et al., 2017, preprint (arXiv:1711.03234)
Kovács G., Zucker S., Mazeh T., 2002, A&A, 391, 369
Kozłowski S., 2017, A&A, 597, A128
Kozłowski S. et al., 2010, ApJ, 708, 927
Leavitt H. S., 1908, Ann. Harvard College Obser., 60, 87
Lomb N. R., 1976, Ap&SS, 39, 447
LSST Science Collaboration et al., 2009, preprint (arXiv:0912.0201)
Majewski S. R. et al., 2017, AJ, 154, 94
Matsunaga N., Feast M. W., Soszyński I., 2011, MNRAS, 413, 223
Moe M., Kratter K. M., Badenes C., 2019, ApJ, 875, 61
Pawlak M., 2016, MNRAS, 457, 4323
Pawlak M. et al., 2016, Acta Astron., 66, 421
Pejcha O., Stanek K. Z., 2009, ApJ, 704, 1730
Pepper J. et al., 2007, PASP, 119, 923
Pietrukowicz P. et al., 2015, ApJ, 811, 113
Pietrzyński G. et al., 2011, ApJ, 742, L20
Pietrzyński G. et al., 2013, Nature, 495, 76
Pojmański G., 1997, Acta Astron., 47, 467
Pojmański G., 2002, Acta Astron., 52, 397
Price-Whelan A. M., Goodman J., 2018, ApJ, 867, 5
Price-Whelan A. M. et al., 2018, AJ, 156, 18
Rodriguez J. E. et al., 2017, ApJ, 836, 209
Rucinski S. M., 1994, PASP, 106, 462

Rucinski S. M., 2004, New Astron. Rev., 48, 703
Scargle J. D., 1982, ApJ, 263, 835
Shapley H., 1931, Harvard College Obser. Bull., 883, 16
Shappee B. J. et al., 2014, ApJ, 788, 48
Skowron D. M. et al., 2018, preprint (arXiv:1806.10653)
Skrutskie M. F. et al., 2006, AJ, 131, 1163
Soszynski I. et al., 2008, Acta Astron., 58, 16
Soszyński I. et al., 2009, Acta Astron., 59, 1
Soszyński I. et al., 2014, Acta Astron., 64, 177
Soszyński I. et al., 2016a, Acta Astron., 66, 131
Soszyński I. et al., 2016b, Acta Astron., 66, 405
Soszyński I. et al., 2017, Acta Astron., 67, 297
Steinmetz M. et al., 2006, AJ, 132, 1645
Storm J., Gieren W., Fouqué P., Barnes T. G., Soszyński I., Pietrzyński G.,
    Nardetto N., Queloz D., 2011, A&A, 534, A95
Thompson T. A. et al., 2018, preprint (arXiv:1806.02751)
Tonry J. L. et al., 2018, PASP, 130, 064505
Trabucchi M., Wood P. R., Montalban J., Marigo P., Pastorelli G., Giradi
    L., 2019, MNRAS, 482, 929
Udalski A., Szymański M. K., Szymański G., 2015, Acta Astron., 65, 1
Watson C. L., Henden A. A., Price A., 2006, Soc. Astron. Sci. Annu. Symp.,
    25, 47
West A. A. et al., 2004, AJ, 128, 426
Wood P. R., Olivier E. A., Kawaler S. D., 2004, ApJ, 604, 800
Wray J. J., Eyer L., Paczyński B., 2004, MNRAS, 349, 1059
York D. G. et al., 2000, AJ, 120, 1579
Yuen Ka-Veng, 2010, Bayesian Methods for Structural Dynamics and Civil
    Engineering. Wiley, New York
Zasowski G. et al., 2013, AJ, 146, 81
Zhao G., Zhao Y.-H., Chu Y.-Q., Jing Y.-P., Deng L.-C., 2012, Res. Astron.
    Astrophys., 12, 723
Zinn J. C. et al., 2017, MNRAS, 468, 2189

This paper has been typeset from a TeX/LaTeX file prepared by the author.